Limnol. Oceanogr., 53(2), 2008, 835–850

Diel carbon monoxide cycling in the upper Sargasso Sea near Bermuda at the onset of spring and in midsummer

Oliver C. Zafiriou[1] *and Huixiang Xie*[2]
Department of Marine Chemistry and Geochemistry, Woods Hole Oceanographic Institution, Woods Hole, Massachusetts 02543

Norman B. Nelson
Institute for Computational Earth System Science, University of California Santa Barbara, Santa Barbara, California 93106-3060

Raymond G. Najjar
The Pennsylvania State University, Department of Meteorology, University Park, Pennsylvania 16802-5013

Wei Wang
Department of Marine Chemistry and Geochemistry, Woods Hole Oceanographic Institution, Woods Hole, Massachusetts 02543

Abstract

Rapid bio-oxidation of carbon monoxide (CO), a photoproduct of dissolved organic matter, results in diel cycles reflecting photochemical–biogeochemical–physical interactions. These cycles were characterized by time-series studies of hydrography, meteorology, insolation, optics, and CO concentration ([CO]). Diel patterns of near-surface [CO] generally varied little seasonally, despite different forcings. In summer 30% of CO was below the mixed layer (ML); ML depths and optics indicate that two-layer photochemistry is common elsewhere. [CO] decayed at similar rates in both isolated layers. In spring CO extended to 150 m, reflecting nocturnal mixing. Cruise-average profiles indicated a shallower ML defined by CO than that defined by density, illustrating short-lived CO's sensitivity to recent mixing. Below the ML, [CO] dropped exponentially with depth on scales controlled by photoproduction in summer but mixing in spring. Mass-balance modeling of diurnal variations in CO column burden (CB) gave similar production rates in summer and spring ($\sim$50 μmol m^{-2} d^{-1} CO), but different bio-oxidation rates, 1.5 $\pm$ 0.2 d^{-1} (summer, 0–50 m) and 0.52–0.66 d^{-1} (spring, 0–200 m). Outgassing averaged 4% of bio-oxidation in summer and 14% in spring. Similar production and differing sinks resulted in different CBs: 39.3 μmol m^{-2} (summer) versus 94.9 μmol m^{-2} (spring). Insolation-normalized CO productions were 1.8 times those in the oligotrophic equatorial Pacific. Improved, well-blanked analyses found [CO] at 200 m always $<$0.1 nmol L^{-1} in summer, and usually in spring. Prior reports of [CO] systematically $\geq$0.2 nmol L^{-1} at depth in well-stratified, oxic blue waters may be high because of method artifacts.

Dissolved carbon monoxide (CO) is produced by the photolysis of chromophoric dissolved organic matter (CDOM) and lost by microbial consumption and outgassing (for CO cycle review, see Zafiriou et al. 2003). Extensive underway mapping to constrain the CO sea–air flux (Conrad et al. 1982; Bates et al. 1995) yielded regional and seasonal mean concentrations of near-surface CO ($[CO]_{surf}$) of 0.19–3.8 (median, 0.99) nmol L^{-1}. These surveys also revealed high supersaturation factors and strong diurnal cycles: $[CO]_{surf}$ often increases two- to fivefold from near-dawn minima to afternoon peaks. Insolation-linked CO formation rates drive diel cycles, but high ($\sim$1 d^{-1}) specific rates of CO loss and vertical mixing largely determine their amplitudes These persistent patterns in underway (non-Lagrangian) data also imply that CO dynamics are often coherent over $\sim$200–500-km scales. These striking features inspired theoretical analyses (Doney et al. 1995, Najjar et al. 1995) and the collection of time-series [CO] profiles for modeling diel-scale CO formation and loss rates (Kettle 1994; Gnanadesikan 1996; Johnson and Bates 1996 [JB96]). Extending this approach, Project DIEL studied the cycles of the short-lived CDOM photoproducts CO, carbonyl sulfide (Cutter et al. 2004), and hydrogen peroxide (Kieber et al. 2001) in two contrasting periods, accompanied by process–rate experiments.

[1] Corresponding author (ozafiriou@whoi.edu).
[2] Present address: Institut des Sciences de la Mer de Rimouski, Université du Québec à Rimouski, 310 Allée des Ursulines, Rimouski, Québec G5L 3A1, Canada.

Acknowledgments

Professor M. Scranton loaned a CO analyzer, P. Novelli recalibrated our CO standard, D. Torres processed the acoustic Doppler current profiler data, and R. Payne provided software for processing meteorological data. We thank our DIEL colleagues and the captains and crews of RV *Endeavor* cruises 327 and 335, and J. Werner, for their cooperation. Reviewers' suggestions notably improved the manuscript.

This work was supported by NSF grants OCE9811208 to O.C.Z., OCE9815179 to R.G.N., and OCE980096265 to N.B.N. H.X. was supported by a Postdoctoral Fellowship from Woods Hole Oceanographic Institution (WHOI), and W.W. by WHOI internal funds.

Although CO distributions were interpreted in many prior papers, the first group publishing a quantitative model was also first to evaluate their methods systematically, recognizing that quantitative interpretability of data and of model–data differences depends critically on data quality. Their surface-water pumping system samples agreed within ~7% with diver-retrieved syringe samples (Johnson 1999), whereas profile reproducibility (on the basis of subsampling single bottles) was ±4.7% at the 0.78 nmol L^{-1} [CO] level and both sampling and analytical blanks were uncertain by 0.20 nmol L^{-1} (JB96). This is 20% of the median Pacific regional mean but 50% in one-sixth of the regions reported, and 100% of the lowest one (Bates et al. 1995). It is not the largest uncertainty for most CO air–sea flux estimates; gas-exchange coefficient parameterizations are even more uncertain. In the water column, modeled CO loss rates of JB96 are ~6–29% too slow if the true blank is 0.2 nmol L^{-1} (JB96). Modeling Atlantic CO data, Kettle (2005) assumed zero sampling blanks, and posited "dark production" to explain [CO] ≥ 0.2 nmol L^{-1} at 50–120 m. Uncertain or unmeasured CO blanks thus seriously limit modeling and interpreting CO data sets.

Before DIEL cruises, we found that CO blanks arise largely from CO outgassing over hours from sunlight-exposed plastics (i.e., Niskin bottles, tubing, and syringe valves) that likely vary on diel timescales, and hence defy robust characterization (see Methods). This paper presents in situ time-series of CO data using refined, validated methods, with blank uncertainties 10-fold lower and reproducibility about twice as good as JB96, along with the ancillary optical, hydrographic, and meteorological data. It summarizes the CO cycle's diel and seasonal trends and analyzes them quantitatively using a vertically unresolved mass conservation model like that of JB96. Incubation-based rates will be presented elsewhere (Xie et al. unpubl. data) and vertically resolved models will clarify the roles of mixing and profile variability (entrainment, detrainment) and provide alternative rate estimates to those derived here (Najjar et al. unpubl. data).

Methods and materials

Study site and sampling strategy—DIEL cruises on the RV *Endeavor* occurred near the Bermuda Atlantic Time-series (BATS) site in August, or "summer" 1999 (day of the year [YD] 218 at 31.37°N, 64.00°W to YD 229 at 31.50°N, 64.03°W) and in March, or "spring" 2000 (YD 77 at 32.01°N, 64.02°W to YD 88 at 32.03°N, 64.01°W). The ship performed daily dawn, afternoon, and dusk hydrocasts, while attempting to follow water parcels ("Lagrangian" mode) by staying within ~0.5–3 km of a spar buoy attached by a 10-m cable to a drogue (four ~0.5-m^2 triangular sails). After the drogue was lost in boisterous weather early in the March cruise, the ship remained near the untethered in situ "optical buoy" or its drift track until the next deployment. Evenings, the ship repositioned near the BATS site using a "dogleg" course to discharge wastes, then sampling water near midnight at the next optical buoy deployment site. Thus data are quasi-Lagrangian in summer, whereas in spring most day's data were acquired separated by ~10–25 km. Frontal passages were monitored with sea surface temperature (SST), salinity, and chlorophyll *a* (Chl *a*) fluorescence data.

Hydrography—Temperature (T) and salinity (S) profiles were measured with a Seabird Electronics (SBE) conductivity–temperature–depth (CTD) system, usually three times per day in August and six times per day in March. Most casts covered 3–200 m. Only downcasts were processed and unrealistic salinity spikes were removed. SST was also measured by (1) an SBE CTD at ~1 m on a retractable floating boom extending ~6 m from the ship's beam (Donaghue et al. 2001), (2) a hull-mounted probe, and (3) an SBE 21 SEACAT thermosalinigraph monitoring the ship's seawater intake at ~4 m. The boom CTD is the most accurate sensor, least influenced by ship warming effects, but was only deployed in calm conditions; the most complete SST data are from the ship probe. Regressions of 30-min averages of the boom CTD versus the ship probe gave $r^2 = 0.962$ in August and 0.999 in March. Mixed-layer depth (ML_D) was calculated using a sensitive criterion, 0.01 kg m^{-3}, to resolve diurnal stratification. Using 0.005 kg m^{-3} usually gave similar results, but also shallower values likely due to noise. Current velocity was measured with an RD Instruments acoustic Doppler current profiler (ADCP) from 9 m to 199 m in 4-m bins. Data, corrected for ship orientation and velocity, were averaged over 30-min intervals. ADCP data gaps totaled ~15 h in August and ~48 h in March.

Meteorology—Data were recorded at 1-min intervals in August (except precipitation) and 0.5-min intervals in March. Relative wind speed and direction were measured 18.6 m above the surface on the main mast with port and starboard R.M. Young model 05103 propeller-and-vane monitors, using the greater value. Absolute wind was computed from relative wind and the ship's velocity and orientation. Precipitation was measured near the wind monitors with a small (~2.5 cm) Innoquest digital gauge (model DRG-6VB) and a 37.5-cm manual gauge (Belfort). An R.M.Young model 50202 digital rain gauge was added near the air temperature sensor in March. Belfort and Innoquest gauges, compared twice in August, agreed within 15%.

CDOM absorption—Spectra were determined at room temperature with a Perkin-Elmer Lambda 18 spectrophotometer, prezeroed with Milli-Q water in 10-cm quartz-windowed cuvettes. This procedure accurately measures absorption coefficients of filtered seawater ≥0.03 m^{-1}, a value typically reached at ~380−420 nm at BATS (Nelson et al. 1998). CDOM spectra samples were filtered through 0.2-μm Nuclepore filters (preflushed with 0.5 liters of Milli-Q water) in an all-glass unit, and stored in the dark at 4°C in acid-washed glass bottles (Qorpak) with polytetrafluoroethylene-lined lids. Spectra, acquired as decadal optical density, were corrected for baseline offsets (Green and Blough 1994) and converted to absorption coefficients, a_{CDOM} (m^{-1}, base e). Values <0.03 m^{-1} were

Table 1. Summary of seasonality of forcings and CO responses. Values are cruise averages; values that average daily means are reported $\pm 1\sigma$ (standard deviation), except that ML depths are grand means. Asterisks denote data from near-surface samples of the 8/99 BATS cruise.

Properties (units)	August cruise	March cruise
Meteorology and insolation		
Wind speed (m s^{-1})	5.1±2.5	9.7±3.2
Precipitation (mm)	46	8
Average day length (h)	13.3	12.0
Clear-sky insolation (MJ m^{-2} d^{-1})	30	24.2
Insolation (MJ m^{-2} d^{-1})	20.9±5.9	17.7±4.6
Range	8.0–26.2	8.5–23.2
Cloudy days; insolation decrease	3/13; −30%	3/13; −26%
TOMS ozone (Dobson units)	282	313
Shortwave UV, 325 nm (kJ m^{-2})	9.29±2	8.2±1.6
Mixed layer status		
Depth at dawn and dusk (m)	21.7±7.4	104.5±54.5
Mean midday depth (m)	7.0±5.4	20.0±20.6
MLT (°C)	27.79±0.085	19.40±0.091
Surface Chl *a* (mg m^{-3})	0.05	0.29
Total Chl *a*, 1−100 m (mg m^{-2})	11.7	35.3
Deep Chl *a* maximum (m)	125	70
Light penetration and absorption K_d (m^{-1}) [e-folding, 1% depth (m)]		
325 nm	0.090 [11, 51]	0.135 [7, 34]
443 nm	0.035 [29, 132]	0.043 [23, 107]
490 nm	0.043 [23, 107]	0.040 [25, 115]
a_{CDOM}(324 nm) (m^{-1})	0.046* (8/99)	0.104
Spectral slope (nm^{-1})	0.033* (8/99)	0.021
Carbon monoxide		
$[CO]_{surf}$ (nmol L^{-1}) [depth (m)]	1.06±0.46 [1] 1.07±0.38 [8]	1.09±0.53 [5]
CO mean column burden (μmol m^{-2})	39.3 (0–50 m)	94.9 (0–200 m)
$[CO]_{air}$ (ppb)	46±9.2	100.3±13.9
CO sea/air saturation factor	33.5±13.8	18.7±9.1
CO sea–air flux (μmol m^{-2} d^{-1})	2.93±2.11	6.54±2.94

extrapolated from shorter-wavelength data using a linear regression of log-transformed data (Blough and Del Vecchio 2002). Because our August CDOM samples, stored frozen, were contaminated (possibly by solvent vapors), giving a_{CDOM} values higher than measured in 5 yr at BATS and exceeding downwelling diffuse attenuation coefficients, a_{CDOM} data measured from *Weatherbird II* 's August BATS cruise was used instead. These data were collected when the vessels were ~30 km apart; when *Weatherbird II* found a K_d (325) (which is quite sensitive to a_{CDOM}) of 0.081, whereas *Endeavor* found 0.082, indicating that they were in the same (optically defined) water mass.

In situ spectral irradiance—Downwelling radiation was measured at the top of the jackstaff with an Eppley Precision Spectral Pyranometer (model PSP), which integrates radiation over 285–2800 nm (E_{air}[285–2800]). Vector downwelling irradiance (E_d, μW cm^{-2} nm^{-1}) was also measured using Satlantic multichannel radiometers (SPMR, profiler; SMSR, continuous surface logger, ~10 m above the sea surface) in 10-nm wavelength bands centered near 324, 340, 379, 411, 443, 490, and 555 nm. The SPMR was deployed from the fantail on a free-fall, hand-recover basis to avoid ship's shadow and to profile slowly (≤1 m s^{-1}) on 174 casts in summer, 92 in spring. In-water data were processed and quality controlled using guidelines of the Bermuda Bio-Optics Project (Siegel et al. 1995*a*; Sorensen and Siegel 2001). Diffuse attenuation coefficients (K_d, m^{-1}) were determined using linear regressions of log-transformed irradiance profiles (Siegel et al. 1995*b*). Daily time–depth fields of downwelling irradiance were prepared for the top 100 m at 10-s intervals by combining surface irradiance records with interpolated K_d profiles after correcting surface irradiances at each wavelength for sea surface reflectance, then extrapolating to depth using interpolated K_d values. Irradiances were converted from energy to photon units using Planck's law. Scalar irradiance, E_s, was then estimated from in situ measurements of E_d and a radiative transfer model, HYDROLIGHT (Mobley 1994). A table of the ratio $E_s : E_d$ was computed using HYDROLIGHT for all relevant wavelengths, depths, and solar zenith angles for each cruise. For this computation, inherent optical properties were estimated using HYDROLIGHT bio-optical model for input values of Chl *a* equal to the surface average for each cruise (Table 1). The resulting conversion factors were applied to in situ E_d irradiance estimated from downwelling in-air irradiance and in situ determinations of K_d. The rate of absorption of photons by CDOM, AQ_{CDOM} (mol photons m^{-3} s^{-1} nm^{-1}; Sorensen and Siegel 2001), was then estimated by convolving E_s with a_{CDOM}. Integrating

with depth gave layer-specifc a_{CDOM} totals (mol photons m^{-2} s^{-1} nm^{-1} [depth interval]$^{-1}$).

CO sampling and analysis—Refined sampling procedures had been tested to minimize artifacts. All profiles were sampled using purpose-built CO-contamination-free 5-liter titanium bottles because polyvinyl chloride (PVC) bottles had been found to contaminate water erratically with 0−0.2 nmol L^{-1} CO, likely due to sunlight-generated CO from PVC (Doherty et al. 2003). In August a single titanium sampler was cast repeatedly (~1.5 h profile^{-1}). In March, six titanium bottles on the CTD rosette were used. ''Surface'' water was sampled amidships by lowering a stainless steel bucket sideways through the interface to minimize turbulence. Immediately after CO samples arrived on deck, duplicates were drawn while protected from light into 100-mL ground-glass syringes with three-way Luer® plastic valves. In August a few samples were contaminated by a stainless steel ball valve on the titanium bottle; replacing it with a stainless steel plug eliminated contamination, which had increased [CO] by 0.092 ± 0.04 L^{-1} at 200 m. On YD 222–224.6, we subtracted 0.092 L^{-1} from samples below 14 m, but zero above, since contamination should be less because of shorter time in bottle. Maximum potential uncertainties from this treatment are 14% overestimates at 8 m and 38% underestimates at 50 m.

A floating boom (Donoghue et al. 2001) was used to continuously sample surface seawater ~6 m away from the hull amidships. Water was pumped from 1 m and at times from 8 m through 316 stainless steel lines at ~550 mL min^{-1} per channel to an automated CO system (Xie et al. 2001) while moving 1–5.3 km h^{-1} to windward to minimize ship-mediated mixing or contamination. A multichannel peristaltic pump with short lengths of ''C-flex'' tubing was housed in a low-light enclosure to eliminate sunlight-plus-tubing photoproduction of CO (Xie et al. 2002). Because of rough seas in March, 1-m water was boom-sampled as feasible to calibrate the primary $[CO]_{surf}$ data stream from the ship's ''clean water'' intake (~4 m, near the bow).

$[CO]_{surf}$ was measured at 4−6 samples h^{-1} by an automated system (Xie et al. 2001). Discrete cast and bucket samples were analyzed manually using a headspace method with 1 : 18 gas : water ratio for CO extraction and a modified RGA3 for its quantification (Xie et al. 2002).

Air samples were drawn at the bow, facing the wind, into water-wet 5-mL glass syringes with plastic three-way valves each morning, afternoon, and evening, and analyzed within minutes by injecting samples into the RGA3 loop in the same manner as gas standards.

CO blanks, standards, precision, and estimated accuracy—Manual analyses were standardized frequently by injection, with a water-wet syringe, of a 1.14×10^{-6} : 1 CO : air ratio (Praxair, 1997). Recalibration at Wood's Hole Oceanographic Institution using dilution by a mass flow controller system of a National Institute of Standards and Technology (NIST)-traceable standard (Scott, ±1%) with a 9.755×10^{-6} : 1 CO : air ratio gave a 1.23×10^{-6} : 1 CO : air ratio for the Praxair tank, the value used here. Reanalysis of this tank at the Climate Monitoring and Diagnostics Laboratory of the National Oceanic and Atmospheric Administration in 2005 by P. Novelli using a vacuum–ultraviolet (UV) fluorescence technique against reference gases of 300–400 parts per billion (ppb) CO by gravimetry (National Oceanic and Atmospheric Administration) and a 9.6 parts per million (ppm) Standard Reference Material (NIST) gave 1.26 and 1.30 ppm, respectively, ~2–6% above the value used here.

The overall blank of the combined sample withdrawal process, syringe contribution, and analysis procedure (but excluding any ''bottle blank'') was 0.03 nmol L^{-1} [CO], as determined by drawing seawater samples by syringe (very similar to the on-deck procedure) from the ''zero-CO'' reservoir of the automated analysis system while it was sparged continuously and rapidly with CO-free air. On the basis of five replicates, the manual analysis precision is ±0.02 nmol L^{-1} ±2% and accuracy better than ±10% (Xie et al. 2002). At 200 m in August we found 0.03 ± 0.01 nmol L^{-1} [CO], equal to the analytical blank (and the lowest, tightest known [CO] values reported), confirming that on-deck sampling using light-protected syringes was artifact-free and that any titanium sampler blank was undetectable. In spring, bucket samples generally agreed with the shallowest bottle samples, whereas in summer they only agreed at midday, although presumably in calm conditions all these samples are valid. Boom system sampling for the automated system was tested on deck at the end of the summer cruise by pumping seawater in daytime in a nearly closed loop to and from a darkened 20-liter carboy that was rapidly sparged with CO-free air. Syringe-sampled water from the pump's output showed no detectable signal artifacts (~ 0.04 ± 0.03 nmol L^{-1}). Standardization of the automated system at ~1 nmol L^{-1} [CO] was described previously (Xie et al. 2001). In spring, automated analyses of 4-m samples from the ship's 4-m system showed 14% lower [CO] (r^2 = 0.98) than samples from 4-m titanium bottles; data were corrected for this loss. Manual samples were routinely drawn and analyzed in duplicate. All-inclusive variability for 130 duplicates from a titanium bottle in summer was evaluated; average [CO] was 0.78 nmol L^{-1} (range 0.02–2.38) and the average pairwise difference was 0.035 nmol L^{-1} or 4.5%, suggesting a standard deviation of the means reported here of ~2.3%.

Gas exchange—Sea–air fluxes were estimated using the formulation of Wannikhof (1992) for short-term wind speeds. CO's Schmidt number was determined following a method similar to that described by Wanninkhof (1992) and then fit (0−30°C) with:

$$Sc_{CO} = -0.0553T^3 + 4.3825T^2 - 140.07T + 2{,}124$$

where T is in °C. $[CO]_{surf}$ values and wind speeds were linearly interpolated at intervals of 5 min so that each [CO] datum corresponds to a wind speed. CO's saturation concentration was computed using the atmospheric data and solubilities given by Wiesenburg and Guinasso (1979). Wind speed was uncorrected from 18.6 m to the standard height, 10 m; correction would decrease CO fluxes by ~10%.

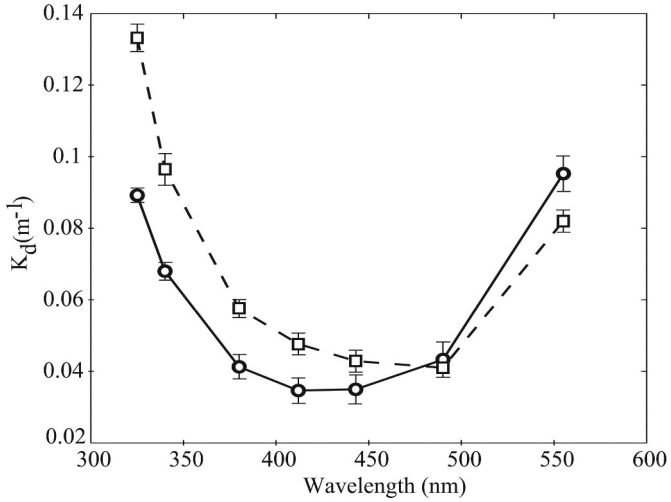

Fig. 1. Spectra of mean diffuse irradiance attenuation coefficients (K_d, m^{-1}) in summer (circles, solid line) and spring (squares, dashed line). Error bars are standard deviations.

CO column burdens (CBs)—These should ideally be derived by integrating profiles to a depth where [CO] is negligible or constant, but in August data limitations usually restricted integrations to 0−50 m. CBs for 0−50 m ($\sum^{50}$CO) and 0−200 m ($\sum^{200}$CO) were obtained by the trapezoid method. When bucket sample data were unavailable, [CO] values from 1 or 4 m were assumed at 0 m. Daily mean CBs were calculated as the arithmetic mean of individual profiles.

Results

Insolation, optics, and light absorption by CDOM—Table 1 shows that March's total insolation was 15% below August's, 12% below in the short-wavelength UV (325 nm), where CO's quantum yield is highest (Kettle 1994; Zafiriou et al. 2003). Differences in [Chl *a*] were much larger: spring was sixfold higher than summer at the surface, threefold integrated over the upper 100 m. Light penetration at <400 nm was ~50% lower in spring (Fig. 1), consistent with higher spring [Chl *a*] (Siegel et al. 1995*b*). The e-folding depth for attenuation of 325-nm light was ~11 m in summer versus 7−8 m in spring, although at 490 nm (near-minimum K_d) the e-folding depth was constant at 23−25 m.

Optically, both cruises sampled periods of subnormal a_{CDOM} and AQ_{CDOM}, a critical variable for CO photoproduction (with quantum yield and insolation). Spring's a_{CDOM} was ~80% of BATS seasonal climatology (Table 1; Nelson et al. 1998; Siegel et al. 2002) and [Chl *a*] was unusually high, resulting in AQ_{CDOM} values moderately below likely BATS AQ_{CDOM} climatology. Summer was markedly more atypical, with extremely low a_{CDOM} (hence, AQ_{CDOM}) (Fig. 2). The August BATS $a_{CDOM}(325)$, the

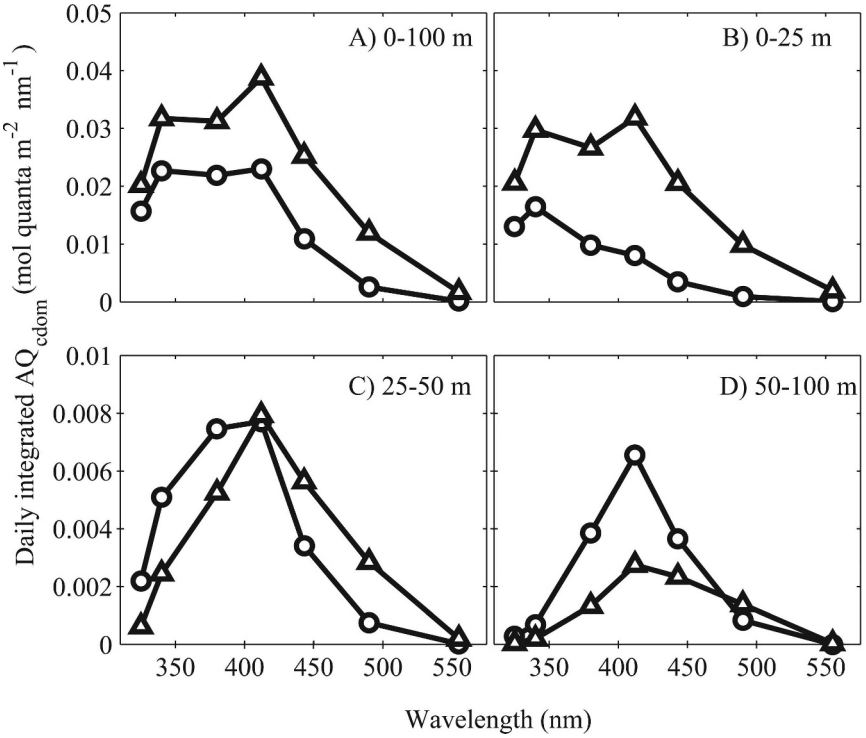

Fig. 2. AQ_{CDOM} spectra (quanta, mol $m^{-2}\,d^{-1}\,nm^{-1}$) in summer (circles) and spring (triangles) integrated over (A) 0–100 m, (B) 0–25 m, (C) 25–50 m, (D) 50–100 m. Note that 0−25 m approximates the summer nighttime ML, as does 0−25 m plus 25–50 m in spring, and that most light is absorbed above 100 m. Summer AQ_{CDOM} was calculated using 8/99 BATS a_{CDOM} spectra. Spring AQ_{CDOM} was calculated using a_{CDOM} samples collected on the DIEL cruise.

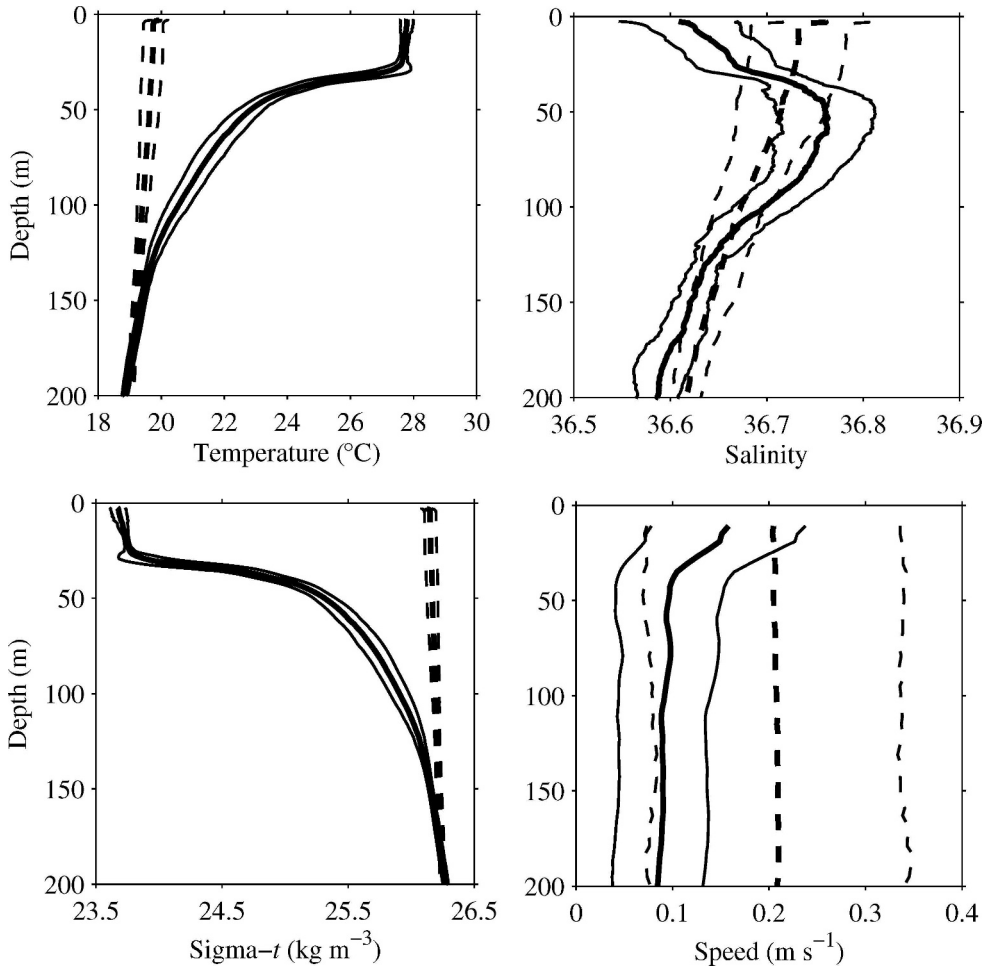

Fig. 3. Mean profiles of temperature, salinity, sigma-*t*, and ADCP horizontal current speeds in summer (dashed lines) and spring (solid lines). Thick lines are means, thin are ±1 SD.

lowest of the preceding 5 yr, lies midway between the June-July-August BATS average and the most transparent waters yet identified (Morel et al. 2005). In spring, $K_d(325)$ trended weakly upward (~0.6% day^{-1} with YD 82 17% above-trend), whereas in summer it was constant (±3%), suggesting that $a_{CDOM}(325)$ did not vary much during this cruise.

CO and ancillary data cruise means and daily-resolved time series—Key averages are given in Table 1 and Fig. 3 and four key high-resolution data time series are shown in Fig. 4, along with the derived quantities ML_D and air–sea exchange flux. As expected, mean *T*, *S*, and density structures contrasted strongly, remaining within known climatological ranges at BATS (Table 1 and Fig. 3; Michaels and Knap 1996; Steinberg et al. 2001). Nighttime ML_D differed by fivefold, and *T* by ~8°C. Transient "surface trapped" layers (Price et al. 1986) occurred at midday on most days in both seasons, as indicated by SST maxima and ML_D minima, ~7 m in summer and 20 m in spring (Fig. 4). Mean currents were higher in spring, but the ML lacked shear then; in summer there was a velocity gradient in the ML (Fig. 3). Spring (vernal equinox) was about twice as windy as summer (1.5 months post solstice). Precipitation events were small (<4 mm) in spring; in summer two events yielded over half of the total: 9.4 mm (YD 218, evening) and 21.1 mm (YD 224, near dawn). Early in spring (YD 77.6–80.3) ML_D increased almost linearly from 35 m to 135 m as SST dropped steadily; concurrently, weak diel $[CO]_{surf}$ cycles rode on a strong downtrend. The other 20 d exhibited clear diel $[CO]_{surf}$ cycles, and the strongest $[CO]_{surf}$ maxima coincided with strong SST maxima (Fig. 4); however, far fewer days exhibited clear SST cycles. The cruises exhibited similar relative variabilities in winds and insolation.

Gas exchange—CO losses (all in μmol m^{-2} d^{-1} in the top 50 m) were close to the 30–45°N seasonal means of Bates et al. (1995): 6.54 versus 5.8 in spring and 2.93 versus 2.9 in summer. The minor role of the exchange sink relative to bio-oxidation, averaging 14% of total CO loss rate in spring and 6% in summer, thus prevents these data from being used to accurately test gas-exchange parameterizations. During windy YD 77–80, outgassing was below average, so that dilution by ML deepening likely dominated the $[CO]_{surf}$ decline. The highest 5% of instantaneous fluxes in spring, 16.6–31.8 μmol m^{-2} d^{-1} (most on YD 82, 84, and 87), and summer, 10.6–16.6 μmol m^{-2} d^{-1} (most

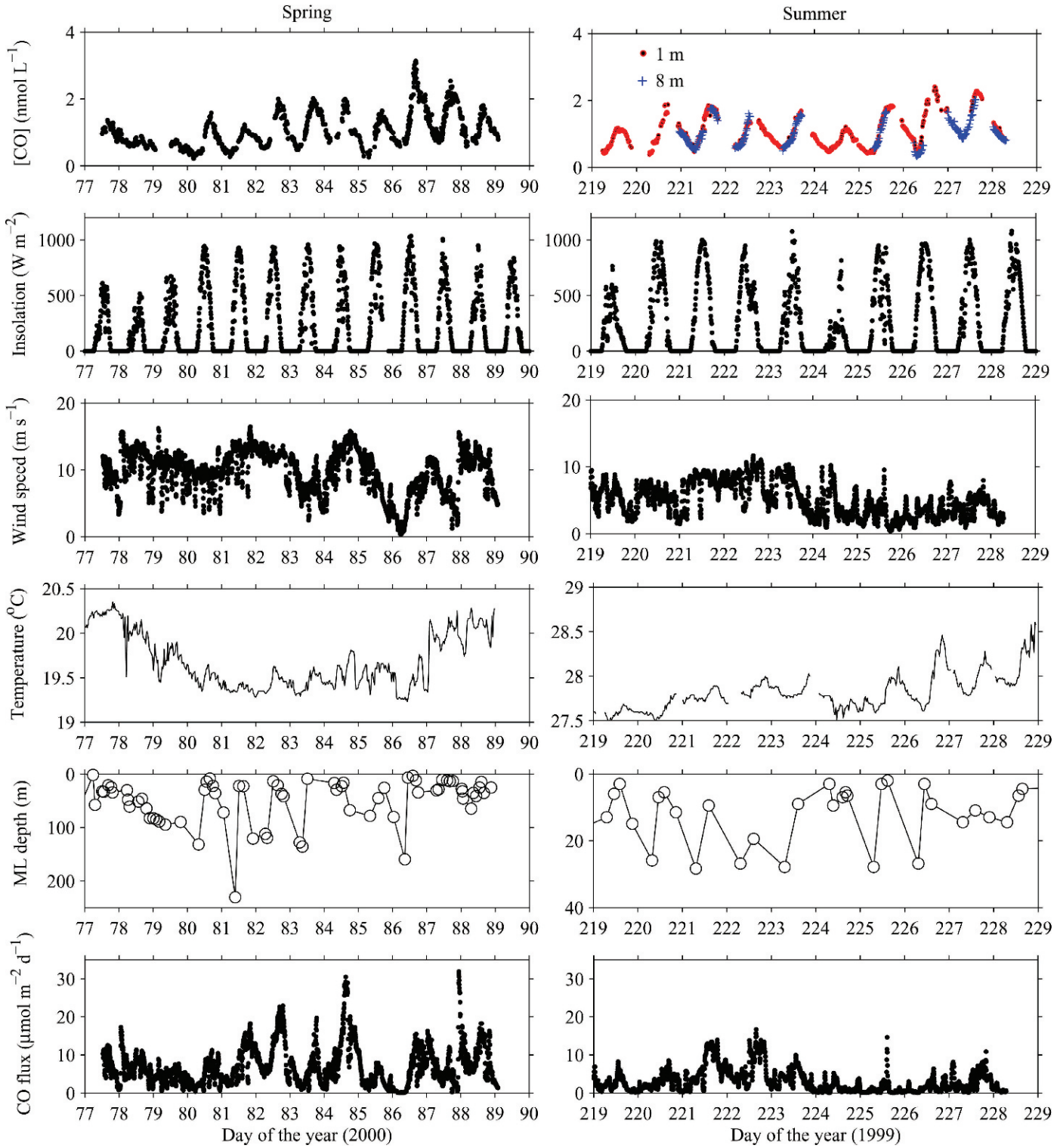

Fig. 4. Spring (left) and summer (right) time-series of near-surface [CO], insolation, wind speed, SST, ML_D, and CO air–sea flux. For daily gas exchanges, see Table 2; for insolation, see Table 3.

on YD 221 and 222), occurred on average at 16:00 h on windy days when $[CO]_{surf}$ was high. Concurrent instantaneous bio-oxidation rates were ~50 and ~150 μmol m^{-2} d^{-1} in spring and summer, so that outgassing was always <40% and <10%, respectively, of the total CO loss rate. Near the interface, $[CO]_{surf}$ was depleted on average in bucket samples relative to 1 m and 5 m [CO] at dawn and dusk, but not at midday. Midday CO production, which is maximal at the surface, apparently balanced near-surface CO losses by outgassing and mixing then.

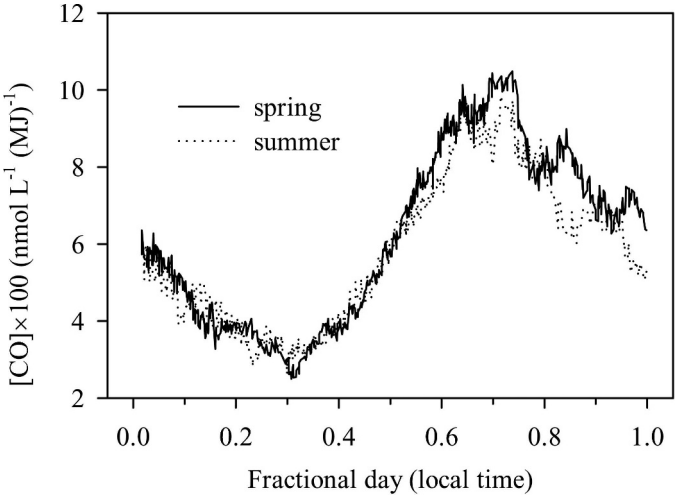

Fig. 5. Composite $[CO]_{surf}$ diel patterns in spring (excluding first 3 d) and summer. Each day's data were divided by that day's insolation to weight sunny and cloudy days equally.

Seasonal and diurnal variability of $[CO]_{surf}$—Cruise means of 1 nmol L^{-1} were similar despite varying climatology. The seasonal invariance of average $[CO]_{surf}$ implies that any lowering of $[CO]_{surf}$ by dilution due to greater spring ML_D was balanced by slower biological losses, higher productions, or both. Normalized to daily insolation to weight days equally, and averaged over days, the mean shapes of spring and summer cycles were nearly superimposable, diverging slightly near sunset, when [CO] dropped sharply by ~0.2–0.3 nmol L^{-1} (Fig. 5). Near dusk, destratification probably dilutes surface-trapped CO with underlying lower-[CO] water (Price et al. 1986). The divergence of averaged diel patterns from sunset to midnight was likely due to nightly repositioning of the ship. A few simultaneous 1- and 8-m $[CO]_{surf}$ data streams showed no gradients even on YD 227, a very low-wind, low-swell day with a clear SST signal, consistent with its ML_D, estimated at >10 m (Fig. 4).

CO profiles—On both cruises, the deepest [CO] are by far the lowest consistently reported. At 200 m above-blank [CO] was never detected in summer ($n = 11$); in spring, it was 0.05 ± 0.03 nmol L^{-1} ($n = 56$); the maximum, 0.24 nmol L^{-1}, occurred on the only day with $ML_D > 200$ m (Fig. 4). A 1-km CO profile to the NW of BATS found CO dropping with depth, detected at 400 m but not below, consistent with a *T* structure that suggested deep mixing (Fig. 6). Time series of dawn, midday, and dusk profiles of *T* and CO in August are shown in Fig. 7. In daytime, [CO] peaked near the surface, decreased rapidly in the top 50 m, and usually reached the blank near 160 m. Systematically less-structured profiles at dawn than at noon and dusk suggest nighttime mixing. With just one titanium sampler, we could not map sub-ML [CO] intensively, but detected diurnal variations at 0−75 m. About 30% of the summer's CB was below the average nighttime ML_D. Since a strong pycnocline inhibited vertical transport then, in situ CO formation occurred at depth, favored by an unusually UV-transparent overlying ML (Fig. 2), perhaps augmented by

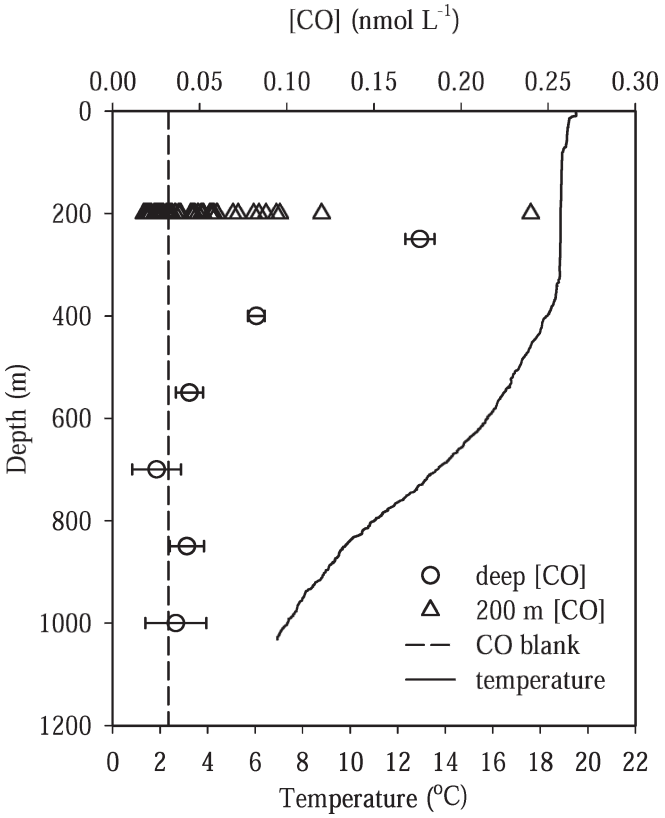

Fig. 6. Deep [CO] profile (circles and error bars) and *T* profile at 33.72°N, 65.38°W, shortly after the ship left BATS in March. Dashed line indicates sampling plus analytical method blank. Triangles show 200-m BATS data in spring. In summer 200 m [CO] was 0.03 ± 0.01 nmol L^{-1}.

slower bio-oxidation, more reactive chromophores, or "dark" production. The latter occurs in estuaries (Xie et al. 2005) and was inferred at BATS (Kettle 2005). Two deeper profiles (not shown) gave YD 227 $\sum^{50}CO : \sum^{200}CO$ ratios of 0.69 (20.5 vs. 29.8 μmol m^{-2}) at dawn but 0.78 (50.2 vs. 64.6 μmol m^{-2}) at dusk. The diel CB difference of 29.7 μmol m^{-2} for $\sum^{50}CO$ and 34.9 μmol m^{-2} for $\sum^{200}CO$ imply (with large uncertainty) that 15% more net CO production may have occurred below 50 m. In March (Fig. 8), CO profiles exhibited smaller gradients in the top 50 m, and CO extended to greater depths, despite lesser light penetration (Table 1; Figs. 1, 2). For example, the 60-m mean [CO] in March was 72% higher than the 50-m mean in August. The CO distribution in March was likely affected by vertical (and possibly horizontal) mixing. Mixing at night was evidenced by nearly constant dawn [CO] profiles as deep as 130 m on YD 83 and 150 m on YD 86 (profiled intensively), consistent with ML_D estimates (Figs. 4, 8).

Persistent seasonal features of CO profiles are clarified by displaying averaged dawn, midday, and dusk casts on logarithmic (base e) scales (Fig. 9). Since outgassing and biological losses are both approximately proportional to [CO], these plots emphasize features that may be interpreted in terms of these processes. Thus overnight loss of an

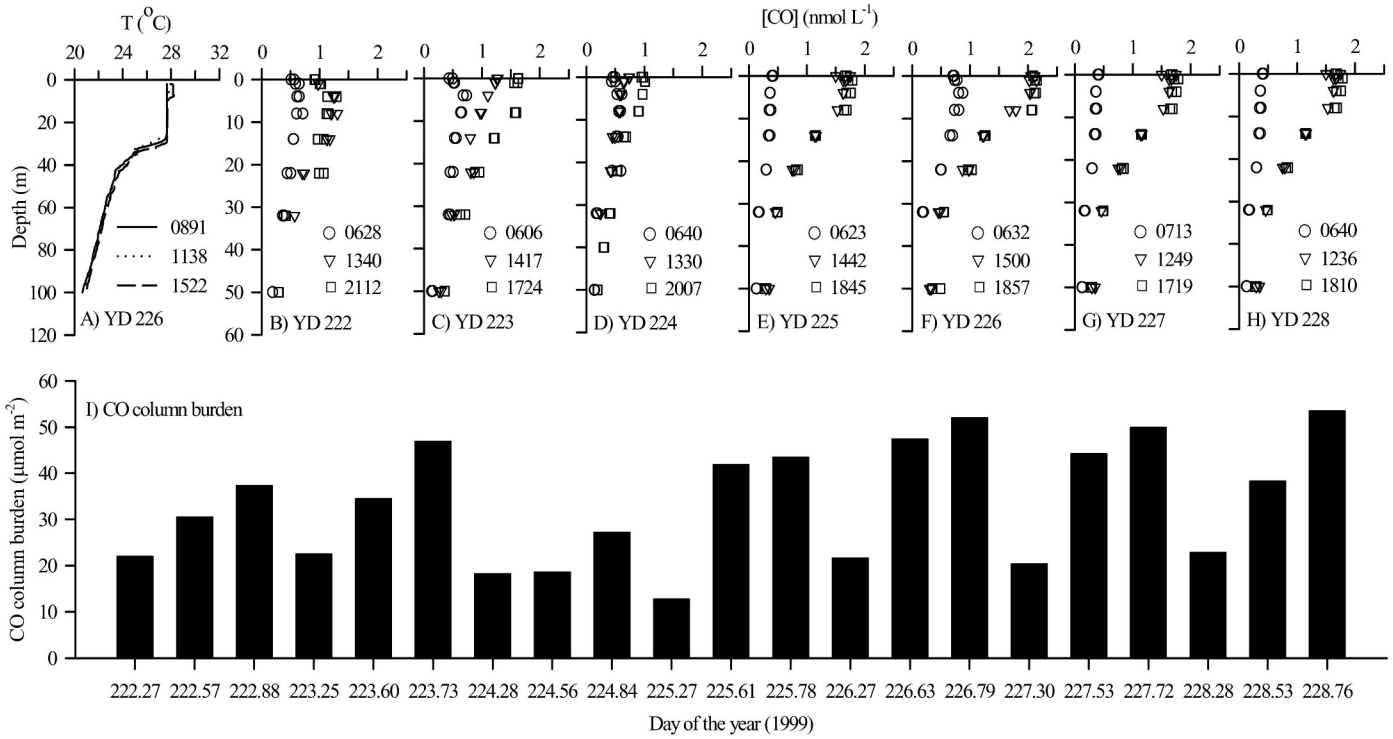

Fig. 7. August 1999: typical (A) temperature and (B–H) CO profiles and 0–50-m CO column burdens. Note different temperature scales in Figs. 7 and 8.

identical *fraction* of [CO] yields a dawn [CO] value offset to the left by a constant distance from the dusk value. To aid in the interpretation of the figure, we estimated a ML depth for CO, ML_{co}, defined by slope breaks. At dawn, mean ML_{co} was less than half of mean ML_D (Fig. 4): ~8 versus 33 m in summer and 40 versus 101 m in spring. In summer, the nighttime decrease was constant over the upper 50 m at 0.8 ln units (a drop of 120%), whereas in spring the decrease (over longer nights) was about 0.7 ln units above dawn's ML_{co} (a 100% decline), gradually decreasing to 0.2 units (overnight decline of 20%) at 100 m. Gas exchange had a minimal influence on these declines, even if limited to ML_{co}; a ~0.1 ln units decrease (a drop of 10%) occurs in summer, whereas in spring, when gas exchange was twice as large but ML_{co} was even larger, the effect was even smaller. The constancy of the fractional overnight CO decline with depth in summer is surprising, given that the long-isolated layers above and below the pycnocline likely differ biogeochemically. In spring, dusk−dawn [CO] declined with depth; also, midday values were much closer to dawn values, whereas in summer they lie closer to dusk values (Fig. 9). Since more than half of net CO production usually occurred by midday (due to slower bio-oxidation at lower [CO] then), the summer pattern is expected, whereas the spring pattern suggests an effect of downward mixing, which is greater at night because of lesser stratification and a longer dusk−dawn than dawn−midday time interval. There may also be a diel cycle in CO bio-oxidation rates (Tolli and Taylor 2005).

If mixing was negligible, the e-folding scales of the linear trends below the ML in Fig. 9 can be interpreted as photoproduction depth scales in regions of similar nighttime decay constants. The summer scale, ~24 m, was consistent with that for penetration of longer-wavelength UV light, whereas the spring scale, ~75 m, implied a K_d of 0.01−0.02 m^{-1}, an impossibly small value at any wavelength (Fig. 1). Thus properties related to CO production and loss both imply that mixing redistributed CO below the ML at night in spring, but not in summer.

CO burdens and their diel cycles—The cruise mean of daily averages in August (0–50 m) was 33.6 μmol m^{-2}, ranging from 21.3 to 40.3 μmol m^{-2} and varying up to 3.4-fold diurnally on YD 225 (Fig. 7). $\sum^{50}CO$ changed little during two especially cloudy intervals; the morning of YD 224, after heavy precipitation, and the late afternoon of YD 225. Although shear in the ML (Fig. 3) suggests relative horizontal motions of ~3 km d^{-1} within it in summer, there is no clear sign of concurrent horizontal effects on CO cycles. Strong diurnal variations in CO CBs also occurred often in March (Fig. 8), when the $\sum^{50}CO$ cruise mean was 46.9 μmol m^{-2}, ~40% higher than in August, and daily values of $\sum^{50}CO$ ranged from 72.2 μmol m^{-2} on YD 80 to 154.5 μmol m^{-2} on YD 86. The March cruise mean $\sum^{200}CO$ is about twice its $\sum^{50}CO$, 94.9 μmol m^{-2}, and similar to $\sum^{120}CO$ at BATS in March 1993 (Kettle 1994). Since in March AQ_{CDOM} (325 and 412 nm) favored deep photoproduction less than in August (Fig. 2), the $\sum^{50}CO$–$\sum^{200}CO$ difference in March again indicated a major role for such effects as downward mixing, slower decay at depth, or other CO sources, since in August ~15% of total CO production was below 50 m.

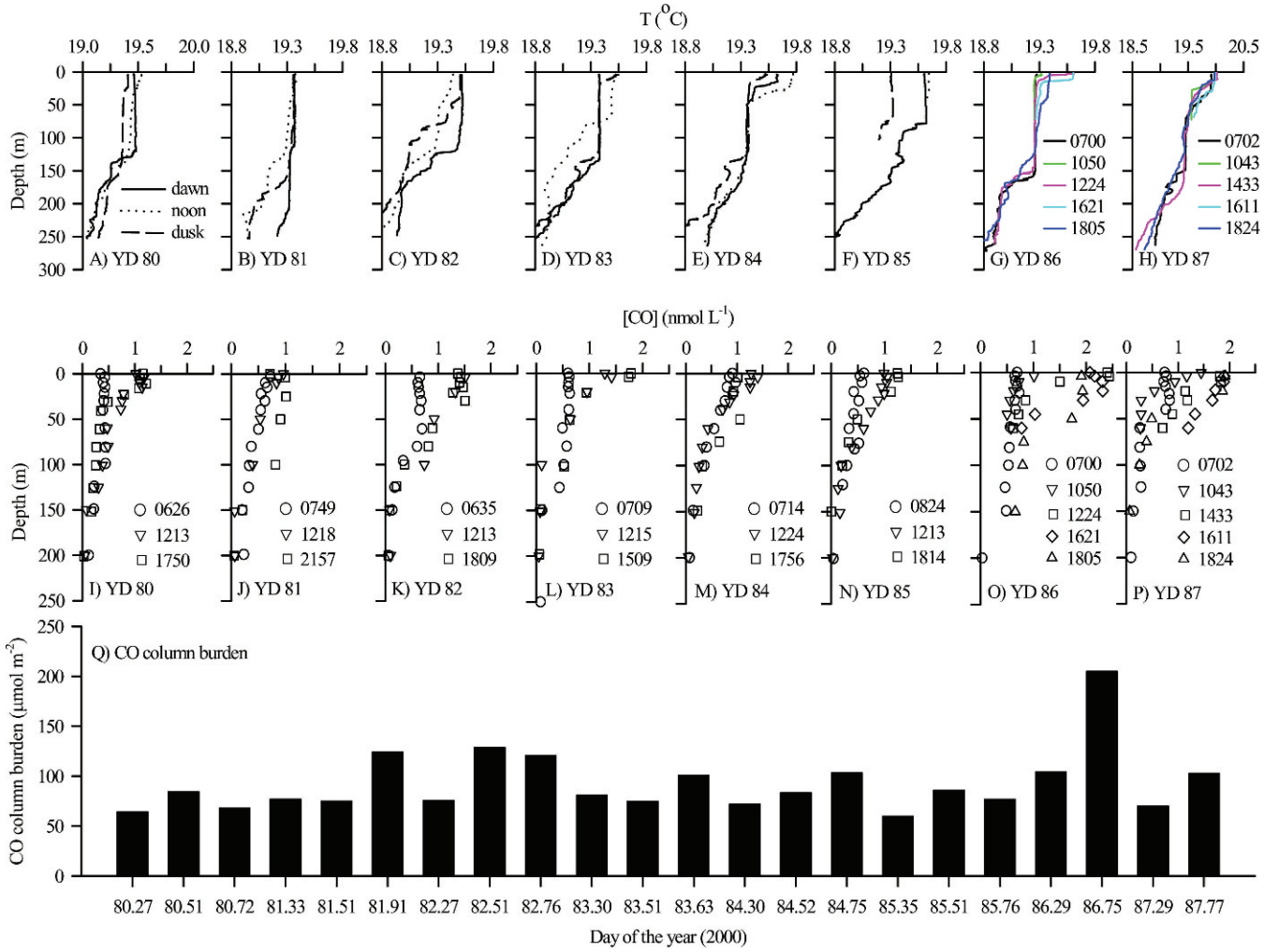

Fig. 8. March 2000: (A–H) temperature and (I–P) CO profiles and 0–200-m CO column burdens.

A non-Lagrangian situation clearly arose after a major drop in wind speed (YD 85.8−86.2, Fig. 4), as shown by large shifts in dawn-to-dawn SST on YD 85−86 (19.90–19.28°C) and YD 86−87 (19.28−19.90°C) that indicate the passage of thermal fronts. YD 86's CO distribution was also exceptional. It began mixed to ~100 m, with a large underlying CO CB (Fig. 8), evolving into the sunniest, calmest spring day, the only one with marked surface trapping, as evidenced by a midday $[CO]_{surf}$ spike (Fig. 4). Its 1224 local time profile indicated that most CO production occurred at ≤20 m, so that increases later in the day at 100 m were unlikely to be down-mixed CO. Best-documented YD 86 (Fig. 8) thus appears unusual in ways that strongly suggest horizontal processes, such as overriding of one recently outcropped water mass by another. In spring there were often strong gradients in SST, [Chl *a*], and nutrients between BATS and waters to the north, signals that were especially strong in 2000 near our cruise dates (Figs. 4 and 5 in Nelson et al. 2004), but velocity shear then was undetectable (Fig. 3) and progressive vector diagrams (that assume flows were horizontally homogeneous) identified no southward trajectories: ~20 km eastward (YD 77−80), 20 km to the southwest (YD 81), 35 km northward (YD 81−82), and 50 km westward (YD 83−86). Thus, although YD 86 cannot be fully understood, it appears highly questionable to model it assuming only vertical processes.

Discussion

Data quality—These data are blanked accurately at the <0.05 nmol L^{-1} level, as shown by an oceanographically consistent low-[CO] deep profile that is in agreement with lab blanks for rapidly degassed water (Fig. 6) and by reproducibly low 200 m [CO] in summer. Several prior studies (Conrad et al. 1982; Jones 1991; Bates et al. 1995) report deep [CO] ~0.2 nmol L^{-1} in well-stratified waters (none systematically lower), values that imply deep-ocean CO CBs of ~800 μmol m^{-2}, 8–20 times $\sum^{50}CO$ or $\sum^{200}CO$ at BATS, and similarly low [CO] values at 50–120 m in March 1993 at BATS were interpreted as requiring dark CO production (Kettle 2005). Since these prior studies did not report sampling and analysis blanks, further work is needed to ascertain whether in 2000 the NW Sargasso's CO cycle was typical (as we believe) or whether a different cycle, perhaps involving "dark production," occurs at other

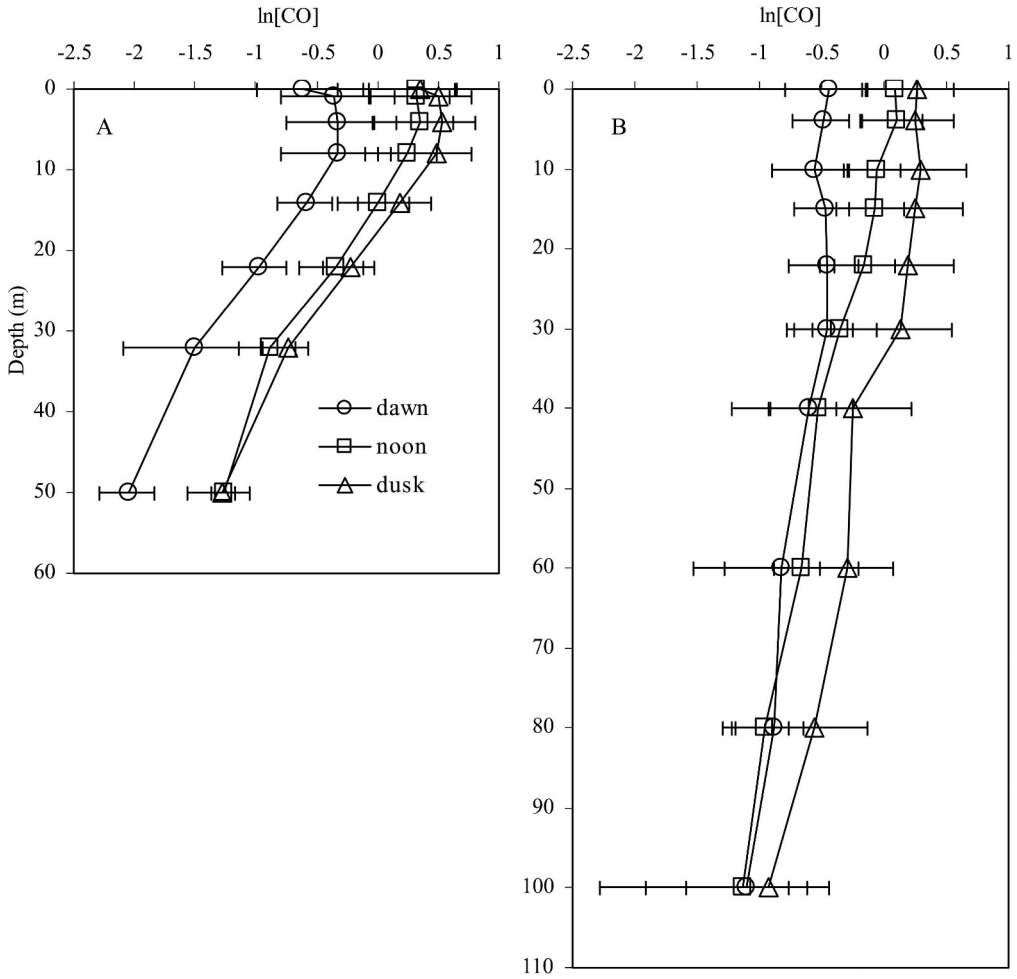

Fig. 9. Logarithmic profiles (base e) of averaged dawn, midday, and dusk [CO]: (A) August 1999, (B) March 2000.

times or places. Titanium bottles useful for resolving these questions are available on loan (Doherty et al. 2003).

Mass conservation model of CO column production and loss—A vertically unresolved model similar to that used by JB96 and Ohta (1997) was used to estimate CO column production and loss rates. Diel cycles of CO CBs are governed by rates of photochemical production, microbial consumption, outgassing, and diffusion across a lower boundary. The model assumes that the net effects of horizontal heterogeneities in [CO] and related properties are insignificant.

This "mass-balance" model is expressed by a conservation equation:

$$\frac{\Delta B}{\Delta t} = \overline{P} - \overline{\lambda} - \overline{F} - \overline{D} \qquad (1)$$

where ΔB is the change in CB of CO over time interval Δt, and $\overline{P}$, $\overline{\lambda}$, $\overline{F}$, and $\overline{D}$ are mean rates of gross column photoproduction, microbial consumption, outgassing, and diffusion over Δt. Diffusion at depth z, D_z, was estimated by multiplying vertical eddy diffusivity, K_z, by d[CO]/dz. K_z values in the open-ocean pycnocline are 0.1−0.2 cm^2 s^{-1} (Watson and Ledwell 2000); conservatively using 0.1−1 cm^2 s^{-1}, estimates of D_{50} could be made three times in August. For example, [CO] at 32–75 m at dusk on YD 227 was fitted with [CO] = 1.10 e$^{-0.0253z}$, giving -d[CO]/dz = 7.9×10^{-3} nmol L^{-1} m^{-1} and downward CO fluxes of 6.8×10^{-3}−6.8×10^{-2} μmol m^{-2} d^{-1}, <1% of the smallest estimated rates. D_{200} in March was also trivial, since then -d[CO]/dz was much smaller. Thus we ignore vertical diffusion in modeling CBs.

Photoproduction at night is zero, so that Eq. 1 simplifies to:

$$\overline{\lambda} = -\frac{\Delta B}{\Delta t} - \overline{F} \qquad (2)$$

Thus from the nocturnal decrease in CB and the sea–air flux, we calculated mean biological consumption rates where feasible using the averages of night-before and night-after data. We assumed that CO microbial loss follows first-order kinetics characterized by a bio-oxidation rate constant, k_{bio}. This treatment simply describes shipboard incubation data (Zafiriou et al. 2003; Xie et al. 2005), although in Atlantic blue water the actual dependence of the biological rate can range from [CO]^0 to [CO]^1 (Xie et al. 2005). As a test, we determined 60 m and 130 m CBs every 2.5 h during YD 78.90–79.3. The data (n = 5) fit both

Table 2. Nocturnal rates and rate constants of CO loss by outgassing and by bio-oxidation on the basis of CO CBs (0–50 m), except for YD 78 (night, 0–60 m; no 50-m data) and the bottom rows (0−200-m average data). ON YD 81 ML_D exceeded 200 m and [CO] at 200 m was 0.24 nmol L^{-1}, so that the dawn CB was underestimated. Nights are denoted by the YD on which they begin. Outgassing rates were converted to rate constants by dividing by (dusk + dawn) average CBs.

	Rates (μmol m^{-2} d^{-1})		Rate constants (d^{-1})	
YD	Outgassing	Bio-oxidation	Outgassing	Bio-oxidation
219	6.97	–	–	–
220	5.33	–	–	–
221	3.38	–	–	–
222	2.86	37.21	0.096	1.27
223	1.41	50.44	0.043	1.67
224	0.65	33.08	0.033	1.74
225	0.59	43.79	0.018	1.40
226	2.35	59.53	0.065	1.77
227	2.80	45.96	0.077	1.33
August mean	2.93	45	0.055	1.5
$\pm 1\sigma$	±2.11	±9.44	±0.029	±0.22
78	1.74	46.12	0.052	1.41
79	2.62	18.88	0.102	0.75
80	4.32	7.75	0.128	0.23
81	8.65	36.05	0.213	0.90
82	7.92	58.31	0.165	–
83	6.4	16.43	0.140	–
84	8.53	27.76	0.222	0.75
85	0.95	40.56	0.024	1.08
86	9.34	98.58	0.142	1.62
87	7.48	–	–	–
88	9.22	–	–	–
0−50-m March mean	6.54	38.94	0.13	0.93
$\pm 1\sigma$	±2.94	±27.39	±0.066	±0.46
0−200-m March mean (all data)	–	–	0.084	0.655
0−200-m March mean (minus YD 86)	–	–	0.089	0.524

linear and exponential regressions well: 0−60 m, [CO] = 42.0 $e^{-1.44\Delta t}$, $r^2 = 0.98$; 0−130 m, [CO] = 69.6 $e^{-1.56\Delta t}$, $r^2 = 0.94$; and 0−60 m, [CO] = $-1.93\Delta t + 41.5$, $r^2 = 0.95$; 0−130 m, [CO] = $-3.47\Delta t + 69.0$, $r^2 = 0.89$, showing mainly that horizontal variability was relatively small. On other days, bio-oxidation rate constants were computed by fitting dusk-to-dawn CB changes with an exponential after accounting for outgassing (Table 2). Outgassing is small, averaging 4% of bio-oxidation in summer and 14% in spring. In August, $\sum^{50}$CO-based rates varied little: 1.50 ± 0.22 d^{-1}, or ± 14%, and were higher than in March, when $\sum^{50}$CO-based rates varied more: 0.93 ± 0.46 d^{-1} or ± 50%. These are only upper limits whenever downward export at night exceeded that in daytime, as seems greatest on YDs 81−83 and 86 (Fig. 4). Therefore, $\sum^{200}$CO values on the basis of the averaged spring dusk minus dawn CBs are also given in Table 2. They are 30−40% smaller than $\sum^{50}$CO-based rates, as expected if they eliminate mixing effects or if rate constants are lower below 50 m. Lower bio-oxidation rate constants in spring than in summer may be due to smaller or genetically or physiologically different microbes (Tolli 2003, Tolli and Taylor 2005), varying cell densities, differing [CO] dependences, or lower rates per cell at lower T (Xie et al. 2005).

Estimating CO photoproduction by assuming equal nighttime and daytime biological rate constants (JB96) gives

$$\overline{P} = \frac{\Delta B}{\Delta t} + \overline{F} + k_{bio}\overline{B} \tag{3}$$

where $\Delta B/\Delta t + \overline{F}$ is net column production, and $\overline{B}$ is the mean CB during the day (average of dawn, midday, and dusk values). Table 3 gives the resulting CO production estimates. In August mean net production on the basis of $\sum^{50}$CO was 27.5 μmol m^{-2} d^{-1} and mean gross production was 51.9 μmol m^{-2} d^{-1}. As noted above, total CO column production may have been up to ~15% higher then. Normalizing to incident solar insolation gives mean net production of 1.33 μmol per megajoule (MJ) and mean gross production of 2.62 μmol MJ^{-1}. Normalizing also decreased the coefficients of variation (31% to 13% [net]; 41% to 24% [gross]), showing that varying insolation caused much of the variation in daily CO production. In March, very similar $\sum^{50}$CO values are given for comparison only; they are not best estimates because of frequent mixing across the 50-m boundary. March mean (−YD 86) $\sum^{200}$CO production was 28.2 μmol m^{-2} d^{-1} (net) or 52.2 μmol m^{-2} d^{-1} (gross), whereas insolation-normalized

Table 3. CO photoproduction rates from 0−50-m mass-balance model, except as noted. Bio-oxidation was calculated by multiplying mean daytime CBs by mean of night-before and night-after bio-oxidation rate constants, data permitting. Production rates were normalized to daily E_{air}(285–2800 nm). 0−200-m means are based on cruise-average dawn and dusk CBs.

YD	Insolation (MJ m^{-2} d^{-1})	Net CO production (μmol m^{-2}) Column	Net CO production (μmol MJ^{-1}) Insolation-normalized	Gross CO production (μmol m^{-2}) Column	Gross CO production (μmol MJ^{-1}) Insolation-normalized
219	12.9	–	–	–	–
220	22.7	–	–	–	–
221	26.3	–	–	–	–
222	22.6	26.16	1.15	48.63	2.14
223	18.9	26.81	1.42	48.83	2.58
224	8.01	9.76	1.22	28.75	3.59
225	21.1	31.36	1.48	57.38	2.72
226	26.2	31.21	1.19	63.30	2.42
227	22.9	36.09	1.58	61.38	2.68
228	24.8	30.92	1.24	55.03	2.21
Summer					
0–50-m mean	20.86	27.47	1.33	51.90	2.62
$\pm 1\sigma$	5.90	±8.48	±0.17	±11.66	± 0.48
77	12.4	–	–	–	–
78	8.52	–	–	–	–
79	12.8	–	–	–	–
80	21.1	19.25	0.91	27.20	1.29
81	21.6	24.21	1.12	36.67	1.70
82	21.8	39.47	1.81	69.12	3.17
83	19.5	24.47	1.32	36.42	1.96
84	16.4	17.94	1.10	29.26	1.79
85	21.1	24.43	1.18	40.77	1.96
86	23.2	69.50	3.00	106.88	4.62
87	18.1	39.20	2.16	79.18	4.37
88	16.3	–	–	–	–
Spring means	17.73	–	–	–	–
	±4.56	–	–	–	–
0−50-m mean	–	32.31	1.58	53.19	2.61
$\pm 1\sigma$	–	±17.11	±0.71	±28.70	±1.28
0−200-m mean					
All data	–	37.35	1.83	68.25	3.36
minus YD 86	–	28.24	1.43	52.19	2.64

values were 1.43 μmol MJ $^{-1}$ and 2.64 μmol MJ^{-1}. Finally, if daytime bio-oxidation was ever negligible, as suggested by some ^{14}CO incubations in summer (Tolli and Taylor 2005), then "net production" (Table 3) actually equaled gross production.

$[CO]_{surf}$ and ML variability—Bates et al. (1995) reported a Pacific daily mean of 0.96 nmol L^{-1} $[CO]_{surf}$, very similar to those at BATS, ~1 nmol L^{-1} (Table 1). However, signals might in principle be gleaned from shorter-term patterns, so that these near-Lagrangian $[CO]_{surf}$ data permit looking for oceanographically interesting properties of the underlying ML as reflected in $[CO]_{surf}$. Diel patterns of $[CO]_{surf}$ were, however, similar on 12 of 13 days in summer, and even between spring and summer >80% of the time. The clearest $[CO]_{surf}$ signature occurred on YD 77.6−80.3, when ML_D increased linearly by ~fourfold as $[CO]_{surf}$ decreased from ~1.2 to typical dawn values of ~0.25 nmol L^{-1} (Fig. 4), dropping exponentially at ~0.6−0.8 d^{-1}. Superimposed daily CO cycles then are unusually weak, 0.3−0.5 versus >1 nmol L^{-1}, due in part to low insolation. (Although $[CO]_{surf}$ dropped at ~0.6−0.8 d^{-1}, YD 78.9−79.3 CB loss rates were ~ 1.5 d^{-1} [see Results]). More subtly, in calm, sunny conditions larger peaks in $[CO]_{surf}$ coincided with the largest SST peaks (Fig. 4), thus signaling unusually strong mid-afternoon stratifications.

Spatiotemporal variability of CO production and its photochemical and remote sensing implications—Modeled gross CO photoproductions at BATS in summer and spring were nearly invariant (51.9 and 52.2 μmol m^{-2} d^{-1}, Table 3). In optically more typical years, seasonal trends in CDOM quality (Nelson et al. 1998) and in [Chl *a*] may favor higher CO production in summer than in spring. The constancy of CO production at BATS in both seasons masks underlying differences in process dynamics, as revealed by AQ_{CDOM} (0–100 m) in the UV and by CO

Table 4. BATS summer and spring AQ_{CDOM} (0–100 m) and CO photoproduction divided by AQ_{CDOM} at selected UV-visible wavelengths. Note that CO production occurs at all wavelengths.

	AQ_{CDOM} (0–100 m) ($10^2 \times$ mol quanta m^{-2} nm^{-1} d^{-1})		Gross CO production: AQ_{CDOM} (μmol CO ($10^2 \times$ mol quanta nm^{-1})) ( ), ratio to summer 325-nm value	
Wavelength (nm)	August	March	August	March
325	1.57	2.13	33.1 (1.000)	24.5 (0.74)
340	2.27	3.27	22.9 (0.69)	16.0 (0.48)
380	2.19	3.37	15.4. (0.47)	15.5 (0.47)
412	2.30	4.33	22.6 (0.68)	12.1(0.37)

production per AQ_{CDOM} (Table 4). These latter ratios are qualitative indices, since production occurs at ~290–450 nm, mostly at ~310–340 nm (Kettle 1994). In summer, UV-region AQ_{CDOM} values are ~two-thirds of those in spring, but summer ratios to CO production indicate more efficient CO production then. Nearly constant productions thus result from roughly compensating shifts in AQ_{CDOM} and AQY_{CO}, the mean UV-region spring AQY_{co} being ~70% of summer's. This estimate is in excellent agreement with an experimental AQY_{co}–T relationship for saline water off the Gulf of the St. Lawrence, which predicts a spring : summer ratio of 74% (Zhang et al. 2006). CO photoproduction efficiency changes at BATS were thus likely dominated by T effects. In contrast, plausible seasonal changes in CDOM molecular composition, which likely affect photochemistry (fresher vs. older, more photobleached CDOM, Nelson et al. 1998), appear to have been relatively minor. The 30% change in photoproduction efficiency is also small compared with changes in bio-oxidation rate constants discussed later.

Modeled gross CO production values in the equatorial Pacific were 41.7 (4°S) and 27.9 (19°S) μmol m^{-2} d^{-1} (JB96), or 80% and 54%, respectively, of the BATS average. Without AQ_{CDOM} values, directly comparing the Pacific sites (JB96) with AQY_{CO} at BATS is impossible. This comparison is important because CO production has been suggested to be a proxy for other CDOM photoproducts, e.g., CO_2 and photolabilized DOM (Miller and Zepp 1995; Moran and Zepp 1997). Also, if CDOM quality varies little, then AQ_{CDOM} estimates, retrievable from remote sensing data and models, can be used to model ocean photochemistry without added AQY_{CO} (or other photoproduct) inputs. Do global, T-adjusted AQYs suffice, or are regional or seasonal parameters needed? Scaling gross CO production to E_{air}(285–2800) values (Table 5) reveals only a 2% spring–summer difference at BATS (in the opposite sense of the 30% difference from the AQ_{CDOM} scaling of Table 4, since at BATS AQ_{CDOM} and AQY_{CO} effects cancelled). The Atlantic–Pacific comparison (Table 5) shows the Pacific sites averaging only two-thirds of the insolation-normalized production at BATS, possibly a significant difference. A better comparison can be made between BATS summer and the Pacific 19°S site because both are in oligotrophic gyres with similar values of key variables that affect AQ_{CDOM} or AQY_{CO} (or both): [Chl *a*] ~0.05 versus 0.07 mg m^{-3}, respectively, and T within 1°C. However, their normalized CO production ratio is 1.8 so that they (and perhaps the two gyres) seem to differ in AQY_{CO}, since this difference is far larger than the ~30% blank-associated uncertainty. More work is clearly needed to clarify this point and to improve proxy and algorithmic applications of CO studies.

Spatiotemporal variability of CO consumption and biogeochemical implications—Modeled summer and spring bio-oxidation rate constant means at BATS varied nearly threefold: 1.53 d^{-1} versus 0.52 d^{-1} (Table 2). Microbial rate changes primarily governed spring–summer CB variations (Table 1) because productions were similar and outgassing was minor. In the equatorial Pacific, biological rate constants of ~0.3−1 d^{-1} were measured (Zafiriou et al. 2003) while 0.09 (4°S) and 0.46 d^{-1} (19°S) were modeled (JB96). Thus Atlantic and Pacific data both suggest that

Table 5. Pacific (JB96) and Atlantic CO photoproductions normalized to E_{air}(285–2800) values on the days on which column CO production was modeled.

N. Atlantic (BATS)		Equatorial S. Pacific	
64°W, 32°N August	64°W, 32°N March	19°S, 149.5°W April	4°S, 140°W December
	Column CO production (μmol m^{-2} d^{-1})		
51.90	52.19 (−YD 86)	27.9	41.7
	E_{air}(285–2800) (MJ m^{-2} d^{-1})		
20.0	19.6	19.3	23.2
	CO production (μmol MJ^{-1})		
2.60	2.66	1.45	1.80
	CO production normalized to BATS average CO production		
0.99	1.01	0.55	0.69

these values are quite variable, and perhaps lower in the Pacific. In summer at BATS, the 0–30-m and 30–50-m layers, presumably isolated for weeks (Michaels and Knap 1996), differ in T, light regime, [CO], and presumably in nutrient regimes and grazing dynamics. Thus, they likely possess distinct microbial ecologies, both generally and with respect to CO metabolism. These layers nevertheless had very similar CO loss rate constants (not rates) (Fig. 9). Since enzymes follow first-order kinetics at low substrate concentrations, similar rate constants suggest that similarly active populations utilized CO. Is this a coincidence, or does CO cycling have (or is it coupled to) an ecological role causing it? Further studies of CO microbiology in two-layer regimes may clarify its role(s), and whether the production rate of CO, suggested as a proxy for CDOM photoproduct formation (Moran and Zepp 1997), can be extended to biological activity. Is CO consumption rate or rate constant also a proxy for the concurrent rate of microbial utilization of bioavailable DOM coproduced with CO by photolysis (Zafiriou 2002)?

Role of mixing depth versus light penetration depth—Wavelength effects on CDOM photobleaching imply that an interacting chromophore array is modified differently under spectrally different illumination (Del Vecchio and Blough 2002, Goldstone et al. 2004), so that the ratio of optical to ML depth is a key parameter, a concept that likely extends to the formation of some other CDOM photoproducts. Interestingly, the summer BATS and 19°S Pacific ratios differ markedly, particularly in the most-active shortwave UV region. The 1% light depths at 325 and 380 nm are 51 m and ~110 m at BATS but ~84 and ~170 m in the Pacific (JB96, Fig. 1), whereas ML_Ds are ~30 and ~90 m, respectively, giving 1% depth : ML_D ratios of ~1.7 and 3.7 at BATS versus 0.9 versus 1.6 in the Pacific. This marked difference may be one factor causing the CO formation efficiency difference noted above, assuming that the sites' CDOM pools are initially identical. Whereas the relatively deep MLs in the equatorial Pacific resulted in one-layer systems, shallow stratification at BATS resulted in a well-developed two-layer system in summer. It is an atypically sited example of a widespread phenomenon, since almost half the sea surface (~30°N–30°S minus equatorial upwellings and coastal waters) exhibits ML_D commonly <25 m (De Boyer Montégut et al. 2004) and relatively low values of a_{CDOM} (Siegel et al. 2002) and [Chl *a*], promoting transparency (Morel et al. 2005). These two-layer photic zones provide common but little-explored natural settings for studying CDOM photochemistry in contrasting light regimes and the system's biogeochemical responses to its photoproducts in differing microbial habitats. To our knowledge, the only prior report of two-layer photochemistry with a sublayer sufficiently developed for quantitative study is that of hydrogen peroxide in the Caribbean (Moore et al. 1993; Sikorski and Zika 1993).

Validation—Modeling produced quite similar (reproducible) results on multiple similar days in each season. Their unknown accuracy may be affected by such unassessed factors as horizontal variability, CB biases from sampling at fixed times and depths, and non-Lagrangian sampling in spring. A companion paper (Xie et al. unpubl. data) will present independent rate estimates from concurrent incubations at BATS. Agreement between modeled in situ data and lab incubation rates addresses the crucial, often-unanswered question of accuracy, whereas disagreements aid in identifying the factors causing inaccuracy.

References

Bates, T. S., K. C. Kelly, J. E. Johnson, and R. H. Gammon. 1995. Regional and seasonal variations in the flux of oceanic CO to the atmosphere. J. Geophys. Res. **100:** 23093–23101.

Blough, N. V., and R. Del Vecchio. 2002. Chromophoric DOM in the coastal environment, p. 509–546. *In* D. A. Hansell and C. A. Carlson [eds.], Biogeochemistry of marine dissolved organic matter. Academic Press.

Conrad, R., W. Seiler, G. Bunse, and H. Giehl. 1982. Carbon monoxide in seawater (Atlantic Ocean). J. Geophys. Res. **87:** 8839–8852.

Cutter, G. A., L. S. Cutter, and K. C. S. Filippino. 2004. Sources and cycling of carbonyl sulfide in the Sargasso Sea. Limnol. Oceanogr. **49:** 555–565.

De Boyer Montégut, C. G., U. Madec, A. S. Fischer, A. Lazar, and D. Iudicone. 2004. Mixed layer depth over the global ocean: An examination of profile data and a profile-based climatology. J. Geophys. Res. **109:** citation number doi 10.1029/2004JC002378 04.

Del Vecchio, R., and N. V. Blough. 2002. Photobleaching of chromophoric dissolved organic matter in natural waters: Kinetics and modeling. Mar. Chem **78:** 231–253.

Doherty, K. D., C. D. Taylor, and O. C. Zafiriou. 2003. Design of a titanium bottle for uncontaminated sampling of carbon monoxide and potentially of other analytes. Deep-Sea Res. (I) **50:** 449–455.

Doney, S. C., R. G. Najjar, and S. Stewart. 1995. Photochemistry, mixing and diurnal cycles in the upper ocean. J. Mar. Res. **53:** 341–369.

Donoghue, T., O. C. Zafiriou, and C. D. Taylor. 2001. Retractable surface-following sampler. Mar. Tech. Soc. **35:** 29–35.

Gnanadesikan, A. 1996. Modeling the diurnal cycle of carbon monoxide: Sensitivity to physics, chemistry, biology, and optics. J. Geophys. Res. **101:** 12177–12191.

Goldstone, J. V., R. Del Vecchio, B. M. Voelker, and N. V. Blough. 2004. A multicomponent model of CDOM photobleaching. Photochem. Photobiol. **80:** 52–60.

Green, S. A., and N. V. Blough. 1994. Optical absorption and fluorescence properties of chromophoric dissolved organic matter in natural waters. Limnol. Oceanogr. **39:** 1903–1916.

Johnson, J. E. 1999. Evaluation of a seawater equilibrator for shipboard analysis of dissolved oceanic trace gases. Anal. Chim. Acta **395:** 119–132.

———, and T. S. Bates. 1996. Sources and sinks of carbon monoxide in the mixed layer of the tropical South Pacific Ocean. Global Biogeochem. Cycles **10:** 347–359.

Jones, R. D. 1991. Carbon monoxide and methane distribution and consumption in the photic zone of the Sargasso Sea. Deep-Sea Res. **38:** 625–635.

Kettle, A. J. 1994. A model of the temporal and spatial distribution of carbon monoxide in the mixed layer. M.S. thesis, Woods Hole Oceanographic Institution/Massachusetts Institute of Technology Joint Program.

———. 2005. Diurnal cycling of carbon monoxide (CO) in the upper ocean near Bermuda. Ocean Model. **8:** 337–367.

Kieber, R. J., W. J. Cooper, J. D. Willey, and G. B. Avery, Jr. 2001. Hydrogen peroxide at the Bermuda Atlantic Time Series Station. Part 1: Temporal variability of atmospheric hydrogen peroxide and its influence on seawater concentrations. J. Atmos. Chem. **39:** 1–13.

Michaels, A. F., and T. Knap. 1996. Overview of the US JGOFS Bermuda Atlantic Time-Series Study and the Hydrostation S program. Deep-Sea. Res. (II) **43:** 157–198.

Miller, W. L., and R. G. Zepp. 1995. Photochemical production of dissolved inorganic carbon from terrestrial organic-matter: Significance to the oceanic organic-carbon cycle. Geophys. Res. Lett. **22:** 417–420.

Mobley, C. D. 1994. Light and water: Radiative transfer in natural waters. Academic Press.

Moore, C. A., C. T. Farmer, and R. G. Zika. 1993. Influence of the Orinoco river on hydrogen peroxide distribution and production in the eastern Caribbean. J. Geophys. Res. **98:** 2289–2298.

Moran, M. A., and R. G. Zepp. 1997. Role of photoreactions in the formation of biologically labile compounds from dissolved organic matter. Limnol. Oceanogr. **42:** 1307–1316.

Morel, A., B. Gentili, H. Claustre, M. Babin, A. Bricaud, J. Ras, and F. Tièche. 2005. Optical properties of the "clearest" natural waters. Limnol. Oceanogr. **52:** 217–229.

Najjar, R. G., D. J. Erickson III., and S. Madronich. 1995. Modeling the air–sea fluxes of gases formed from the decomposition of dissolved organic matter: Carbonyl sulfide and carbon monoxide, p. 106–132. *In* R. G. Zepp and C. H. Sonntag [eds.], The role of nonliving organic matter in the earth's carbon cycle: Report of the Dahlem Workshop on the Role of Nonliving Organic Matter in the Earth's Carbon Cycle. J. Wiley.

Nelson, N. B., D. A. Siegel, and A. F. Michaels. 1998. Seasonal dynamics of colored dissolved material in the Sargasso Sea. Deep-Sea. Res. (II) **45:** 931–957.

———, D. A. Siegel, and J. A. Yoder. 2004. The spring bloom in the northwestern Sargasso Sea: Spatial extent and relationship with winter mixing. Deep-Sea. Res. (II) **51:** 987–1000.

Ohta, K. 1997. Diurnal variation of carbon monoxide concentration in the Equatorial Pacific upwelling region. J. Oceanogr. **53:** 173–178.

Price, J. F., R. A. Weller, and R. Pinkel. 1986. Diurnal cycling: Observations and models of the upper ocean response to diurnal heating, cooling, and wind mixing. J. Geophys. Res. **91:** 8411–8427.

Siegel, D. A., S. Maritorena, N. B. Nelson, D. A. Hansell, and M. Lorenzi-Kayser. 2002. Global distribution and dynamics of colored dissolved and detrital organic materials. J. Geophys. Res. **107:** 3228, doi: 10.1029/2001JC000965.

———, A. F. Michaels, J. C. Sorensen, M. C. O'Brien, and M. A. Hammer. 1995*b*. Seasonal variability of light availability and utilization in the Sargasso Sea. J. Geophys. Res. **100:** 8695–8713.

———, M. C. O'brien, J. C. Sorensen, D. A. Konnoff, and E. Fields. 1995*a*. BBOP Data Processing and Sampling Procedures, ver. 1. U.S. Joint Global Ocean Flux Study Planning and Coordination Office, Woods Hole, MA.

———, T. K. Westberry, and J. C. Ohlmann. 1999. Cloud color and ocean radiant heating. J. Climate **12:** 1101–1116.

Sikorski, R. J., and R. G. Zika. 1993. Modeling mixed-layer photochemistry of H2O2: Physical and chemical modeling of distribution. J. Geophys. Res. **98:** 2329–2340.

Sorensen, J. C., and D. A. Siegel. 2001. Variability of the quantum yield for carbon assimilation in the Sargasso Sea. Deep-Sea Res. II **48:** 2005–2035.

Steinberg, D. K., C. A. Carlson, N. R. Bates, R. J. Johnson, A. F. Michaels, and A. H. Knap. 2001. Overview of the US JGOFS Bermuda Atlantic Time-series Study (BATS): A decade-scale look at ocean biology and biogeochemistry. Deep-Sea Research (II) **48:** 1405–1447.

Tolli, J. D. 2003. Identity and dynamics of the microbial community responsible for carbon monoxide oxidation in marine environments. Ph.D. thesis. WHO/MIT Joint Program.

———, and C. D. Taylor. 2005. Biological CO oxidation in the Sargasso Sea and in Vineyard Sound, Massachusetts. Limnol. Oceanogr. **50:** 1205–1212.

Wanninkhof, R. 1992. Relationship between windspeed and gas exchange over the ocean. J. Geophys. Res. **97:** 7373–7382.

Watson, A. J., and J. R. Ledwell. 2000. Oceanographic tracer release experiments using sulphur hexafluoride. J. Geophys. Res. **105:** 14325–14337.

Wiesenburg, D. A., and N. L. Guinasso, Jr. 1979. Equilibrium solubilities of methane, carbon monoxide, and hydrogen in water and sea water. J. Chem. Eng. Data **24:** 356–360.

Xie, H., S. S. Andrews, W. R. Martin, W. Wang, C. Taylor, and O. C. Zafiriou. 2002. Validated methods for sampling and headspace analysis of CO in seawater. Mar. Chem. **77:** 93–108.

———, O. C. Zafiriou, T. P. Umile, and D. J. Kieber. 2005. Biological consumption of carbon monoxide in Delaware Bay, NW Atlantic and Beaufort Sea. Mar. Ecol. Prog. Ser. **290:** 1–14.

———, O. C. Zafiriou, W. Wang, and C. D. Taylor. 2001. An automated segmented-continuous-flow-equilibration method for in-situ measurement of dissolved carbon monoxide in natural waters. Environ. Sci. Technol. **35:** 1475–1480.

Zafiriou, O. C. 2002. Sunburnt organic matter: Biogeochemistry of light-altered substrates. Limnol. Oceanogr. Bull. **11:** 69–74.

———, S. S. Andrews, and W. Wang. 2003. Concordant estimates of oceanic carbon monoxide source and sink processes in the Pacific yield a balanced global "blue water" CO budget Global Biogeochem. Cycles **17:** 1015, doi: 10.1029/2001GB001638.

Zhang, Y., H. Xie, and G. Chen. 2006. Factors affecting carbon monoxide photoproduction in the St. Lawrence estuarine system (Canada). Environ. Sci. Technol. **40:** 771–777.

Received: 3 April 2007
Accepted: 11 October 2007
Amended: 1 November 2007